Journal of Statistical Physics, Vol. 118, Nos. 5/6, March 2005 (© 2005)
DOI: 10.1007/s10955-004-2687-4

Lyapunov Modes in Hard-Disk Systems

Jean-Pierre Eckmann,[1,2] Christina Forster,[3] Harald A. Posch[3] and Emmanuel Zabey[1]

Received April 12, 2004; accepted December 2, 2004

We consider simulations of a two-dimensional gas of hard disks in a rectangular container and study the Lyapunov spectrum near the vanishing Lyapunov exponents. To this spectrum are associated "eigen-directions", called Lyapunov modes. We carefully analyze these modes and show how they are naturally associated with vector fields over the container. We also show that the Lyapunov exponents, and the coupled dynamics of the modes (where it exists) follow linear laws, whose coefficients only depend on the density of the gas, but not on aspect ratio and very little on the boundary conditions.

KEY WORDS: Nonlinear dynamics; Hamiltonian dynamics; extended systems; Lyapunov spectrum.

1. INTRODUCTION

In this paper, we study the Lyapunov spectra of two-dimensional hard-disk systems and, in particular, the associated "Lyapunov modes".[1,2] Recently, this topic has received considerable attention,[3–8] and a lot of progress has been made in the understanding of the issues involved. In the present work, we synthesize and expand the results found earlier. In particular, we completely classify these modes and give a simple interpretation of their dynamics, in particular for systems with arbitrary aspect ratio. We furthermore present new simulations in support of this classification.

The Lyapunov *exponents* describe the rates of exponential growth, or decay, of infinitesimal phase-space perturbations, and are taken to be

[1]Département de Physique Théorique, Université de Genève, Switzerland; e-mail: jean-pierre.eckmann@physics.unige.ch
[2]Section de Mathématiques, Université de Genève, Switzerland.
[3]Institute for Experimental Physics, University of Vienna, Austria.

ordered according to $\lambda^{(1)} > \lambda^{(2)} > \cdots > \lambda^{(\ell)}$.[4] Because of the Hamiltonian nature of the problem, they come in conjugate pairs,

$$\lambda^{(j)} = -\lambda^{(\ell-j+1)} \ .$$

As is well-known, 0 is always a Lyapunov exponent for such systems and therefore, as a consequence, ℓ is odd. At any point ξ in phase space, the tangent space $TX(\xi)$ decomposes into a sum

$$TX(\xi) = E^{(1)}(\xi) \oplus \cdots \oplus E^{(\ell)}(\xi) \ ,$$

where $E^{(j)}(\xi)$ is the (linear) space of those perturbations of the initial condition ξ whose growth rate is $\lambda^{(j)}$ for the forward dynamics, and $-\lambda^{(j)}$ for the time reversed dynamics. This decomposition is called the Oseledec splitting.

We say that the Lyapunov exponent $\lambda^{(j)}$ is d-fold degenerate if $\dim E^{(j)}(\xi) = d$. It should be noted that, when the Lyapunov exponents are d-fold degenerate, only the subspace corresponding to all d of them is well defined[5]. The main idea of our full classification of Lyapunov exponents and their modes is based on this simple observation.

The Lyapunov *modes* are defined as follows: at time $t = 0$, we take n orthogonal tangent vectors at ξ and, by applying to them the tangent-space dynamics[6] for a long-enough time t, map them onto n vectors which, generally, are not orthogonal but still span an n-dimensional subspace $S_n(t)$. If, instead of n, we consider only $n-1$ vectors, they similarly span an $n-1$ dimensional subspace $S_{n-1}(t)$, such that $S_{n-1}(t) \subset S_n(t)$. The *Lyapunov mode* is a unit vector in $S_n(t)$ which is orthogonal to the space $S_{n-1}(t)$. We will give a precise definition in the next section, explain the algorithmic aspects in Section 3.1 and relate the modes to Oseledec's subspaces in Section 3.2

The study of Lyapunov modes[2,8] has revealed interesting spatial structures which we will define later but which come in two types: *localized structures* associated with the large positive and negative Lyapunov exponents, and *smooth delocalized structures* of wave-like type for exponents close to zero.[1,8] The exponents associated with the latter are degenerate and give rise to a step-like appearance of the Lyapunov spectrum as is shown, for example, in Fig. 1.

[4] ℓ is at most the dimension of the phase space. Note that $\lambda^{(j)}$ stands for *different* Lyapunov exponents, while we will use λ_i when we consider them with multiplicity.

[5] In this, and many other aspects, the theory of Lyapunov exponents is very similar to that of matrices.

[6] See Section 2 for details.

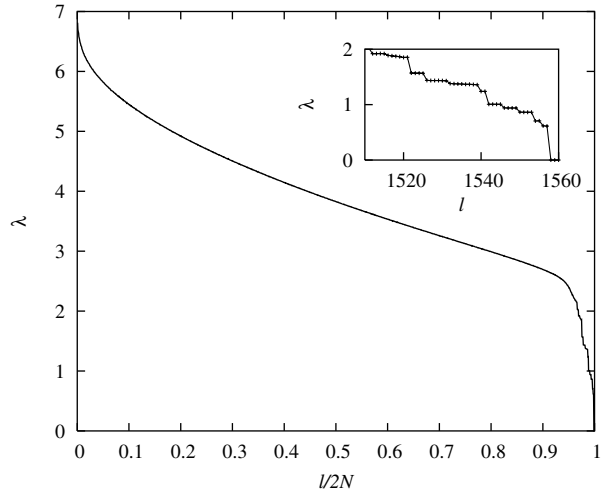

Fig. 1. Lyapunov spectrum for $N = 780$ hard disks at a density $\rho \equiv N/(L_x L_y) = 0.8$ in a rectangular periodic box with an aspect ratio $L_y/L_x = 0.867$. The insert provides a magnified view of the mode regime. l is the Lyapunov index numbering the exponents.

The discovery of these structures has led to several studies[3–7] which go some way in explaining their origin and their dynamics. In this paper, we show how they are related to the symmetries of the container in which the particles move (including the boundary conditions). At the same time we obtain a classification of the degeneracies of the Lyapunov exponents near zero. This classification allows to view the so-called "mode dynamics" from a new geometrical perspective.

The paper starts with a summary of results, passes through a precise definition of the Lyapunov modes, and then describes them as vector fields. In Section 4 these vector fields are classified, and their dynamics is studied in Section 5. The last sections deal with the density dependence and with possible hydrodynamic aspects.

2. NOTATION AND SUMMARY OF RESULTS

We consider a system of N hard disks of diameter σ and mass m moving in a two-dimensional rectangular container with sides of lengths L_x and L_y. At this point, we do not need to specify the boundary conditions.[7] The phase space of such a system is

$$X = \mathbf{R}^{2N} \times ([0, L_x] \times [0, L_y])^N,$$

[7]We will consider reflecting and periodic boundary conditions.

and a phase point ξ in X is

$$\xi = (p, q) = (p_1, \ldots, p_N, q_1, \ldots, q_N).$$

When necessary, we will write $q_i = (q_{i,x}, q_{i,y})$ to distinguish the two position components of particle i, and similarly for the momenta. The dynamics of the system is that of free flight, interrupted by elastic binary collisions. If ξ_0 is the state of the system at time 0, then $\xi_t = \Phi^t(\xi_0)$ is the state at time t, where $\Phi^t : X \to X$ defines the flow.

Apart from issues of differentiability, which will be addressed when we describe the numerical implementation in Section 3, we call $D\Phi^t$ the tangent flow. Informally speaking, it is a $4N \times 4N$ matrix of partial derivatives and can be thought of as the first-order term (in ε) in an expansion of the perturbed flow,

$$\Phi^t(\xi_0 + \varepsilon\delta\xi) = \Phi^t(\xi_0) + \varepsilon\, D\Phi^t\big|_{\xi_0} \cdot \delta\xi + \mathcal{O}(\varepsilon^2).$$

The vector $\delta\xi$ lies in the tangent space TX (at ξ_0) to the manifold X; in our case $TX(\xi_0) = \mathbf{R}^{4N}$. We next invoke the multiplicative ergodic theorem of Oseledec[9,10]. To do so, we need ergodicity of the Liouville measure. Without further knowledge, we assume this for our case.

Theorem. There exist an integer ℓ and numbers $\lambda^{(j)}$, $j = 1, \ldots, \ell$ such that for almost every $\xi \in X$ (with respect to the Liouville measure) the tangent space splits into

$$TX(\xi) = E^{(1)}(\xi) \oplus E^{(2)}(\xi) \oplus \cdots \oplus E^{(\ell)}(\xi),$$

with the property:

$$\lim_{t \to \pm\infty} \frac{1}{|t|} \log \| D\Phi^t\big|_\xi \, \delta\xi \| = \pm\lambda^{(j)}$$

for $\delta\xi \in E^{(j)}(\xi)$. The spaces $E^{(j)}(\xi)$ are covariant: $D\Phi^t\big|_\xi \, E^{(j)}(\xi) = E^{(j)}(\Phi^t(\xi))$.

The dimension $d^{(j)}$ of $E^{(j)}(\xi)$ is called multiplicity of the exponent $\lambda^{(j)}$. In general the $E^{(j)}$ are not orthogonal to each other.

We also use the notation

$$\lambda_1 \geqslant \lambda_2 \geqslant \cdots \geqslant \lambda_i \geqslant \cdots \geqslant \lambda_{4N}$$

to denote the Lyapunov exponents repeated with multiplicities, where the index is referred to as the Lyapunov index. This notation is more adequate for describing numerical methods of measurement, in which tangent-space dynamics is probed by a set of vectors. With these notations the relation between the $\lambda^{(j)}$ and the λ_i is given by

$$\lambda^{(j)} = \lambda_{f^{(j-1)}+1} = \cdots = \lambda_{f^{(j)}},$$

where $f^{(j)} = d^{(1)} + \cdots + d^{(j)}$. Choosing $j \in \{1, \ldots, \ell\}$ and letting $F^{(j)} = E^{(1)} \oplus \cdots \oplus E^{(j)}$, we define the $d^{(j)}$ Lyapunov modes associated with $\lambda^{(j)}$ as any orthogonal spanning set of the space

$$M^{(j)} \equiv (F^{(j-1)})^{\perp} \cap F^{(j)}. \tag{1}$$

A finer decomposition of this spanning set will be obtained when we describe the algorithm used, see Section 3.1. The subspaces $M^{(j)}$ are very similar to the subspaces $E^{(j)}$: they have the same dimension and also satisfy $F^{(j)} = M^{(1)} \oplus \cdots \oplus M^{(j)}$. However, they are not identical, because of the orthogonality constraint in (1). This will be explained in Section 3.2.

In this summary, we focus on rectangular boxes with *periodic* boundary conditions. Narrow systems ($L_y < 2\sigma$) or systems with reflecting boundaries have a very similar Lyapunov spectrum, but some exponents found in the periodic case are either absent, or appear with smaller multiplicities. We shall treat such systems in Section 4.3 but concentrate, until then, on the "general" periodic case. However, it should be noted that systems with reflecting boundaries give important information on the relation between the vanishing and the small Lyapunov exponents (see Ex. 3 below).

The Lyapunov exponents near zero are found to be proportional to the wave numbers of the system,

$$k_{(n_x,n_y)} = \sqrt{\left(\tfrac{2\pi}{L_x} n_x\right)^2 + \left(\tfrac{2\pi}{L_y} n_y\right)^2}\ , \quad n_x, n_y = 0, 1, \ldots . \tag{2}$$

Remark. This result, as well as all results mentioned below, are to be understood in the limit of an infinite number of disks, at fixed density. In particular, we omit higher order terms (in k) in most of our statements.

The Lyapunov exponents have the following properties:

Lyapunov Spectrum: For gases of hard disks, the Lyapunov exponents near zero are fully determined by two (positive) constants, c_{L} and c_{T}. For small-enough $\mathbf{n}=(n_x, n_y)$, these exponents lie on two straight lines.[8]

(1) Transverse branch (T): $\lambda = \pm c_{\mathrm{T}} k_{\mathbf{n}}$, with multiplicity 4 (2 if either n_x or n_y is zero)

(2) Longitudinal branch (L): $\lambda = \pm c_{\mathrm{L}} k_{\mathbf{n}}$, with multiplicity 8 (4 if either n_x or n_y is zero)

The multiplicities of both branches will be explained by simple geometric observations in Section 4.2. While the linear laws resemble the square roots of the eigenvalues of a Laplacian in the box, we have no explanation beyond those already given in ref. 3. (The square root is related to the symplectic nature of the problem.) Additional degeneracies arise in square systems and may accidentally appear also for specific aspect ratios L_y/L_x.

We next explain how to visualize a mode.[8,11] Fix $\xi=(p,q)\in X$, and let $\delta\xi$ be a Lyapunov mode of $TX(\xi)$. The vector $\delta\xi=(\delta p, \delta q)$ has $4N$ components, $2N$ associated with the momenta and $2N$ with the positions. Consider, for example, the q components, $\delta q_1, \ldots, \delta q_N$, where each δq_j is in $\mathbf{R}^2$ (corresponding to the infinitesimal x and y displacements of q_j, $j=1, \ldots, N$). By drawing the perturbation vectors δq_j at the positions q_j of the particles in the box, one obtains a field of vectors as is shown in Fig. 2. For dense-enough fluids we obtain a vector field in every point of the box by interpolating between the particles.

It has been observed that for those Lyapunov exponents close to zero, this vector field is well approximated by trigonometric functions of the spatial coordinates x and y.[1,8] In particular, the number of nodes (n_x, n_y) of the vector field determines a wave number $k_{\mathbf{n}}$. We then say that $\delta\xi$ is a mode of wave number $k_{\mathbf{n}}$. Our second main result is:

Mode Classification: The subspaces $M^{(j)}(\xi)$ (defined in (1)) belonging to Lyapunov exponents $\lambda^{(j)}$ close to zero fall into two categories:

(1) Transverse branch: modes associated with a Lyapunov exponent $\pm c_{\mathrm{T}} k_{\mathbf{n}}$ are divergence-free periodic fields of wave number $k_{\mathbf{n}}$.

[8] For both the longitudinal and transverse modes the linear k dependence of λ is only the first term of an expansion in powers of k[8], $\lambda = ck + c_2 k^2 \cdots$. For positive λ, c_2 is positive, but small. For a second order calculation in k, see ref. 7.

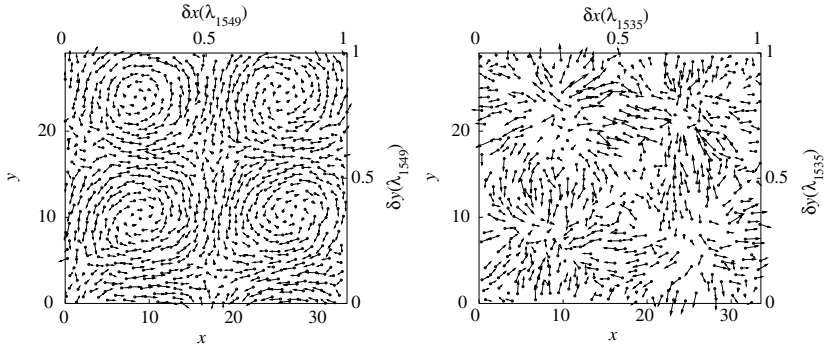

Fig. 2. Modes for the 780-disk system with periodic boundaries characterized in Fig. 1. Left: Transverse mode T(1,1) belonging to λ_{1549}. Right: Longitudinal mode for λ_{1535} belonging to an LP pair LP(1,1).

(2) Longitudinal branch: The modes associated with the Lyapunov exponent $\pm c_{\mathrm{L}} k_{\mathbf{n}}$ are of two types:

(i) Half of them are irrotational periodic vector fields of wave number $k_{\mathbf{n}}$ (called L-modes);

(ii) The others are scalar modulations with wave number $k_{\mathbf{n}}$ of the momentum field, (called P or momentum modes).

The L and the P-modes turn out to be paired: the P-mode has components $p_i A(q_i)$ and the corresponding L-mode has components $\nabla A(q_i)$, where A is a scalar function, see Eq. (9). In the following, we refer to an L-mode and its corresponding P-mode as an LP *pair*. We will give more details on this relation below. Results in this direction have been obtained in refs. 4,6,7.

An interesting question, which is related to some hydrodynamic aspects of the fluid, is an apparent propagation of the L and P-modes in physical space. It is a consequence of the motion of the tangent vectors in the subspaces $M^{(j)}(\xi_t)$, to which we refer as *mode dynamics*. It will be described in detail in Section 5. We note that this motion is not only determined by the tangent flow, but also by the re-orthonormalization process part of the algorithm for the simulation. Mode dynamics was observed early on,[2,11] but attempts to compute the propagation velocities are still scarce and, at present, only work for low densities.[5,7] Here, we give a more precise definition and provide numerical results.

Mode Dynamics: In an $M^{(j)}$ space of Longitudinal and P-modes, the mode dynamics couples LP pairs. When restricted to the two-dimensional

subspace spanned by a given LP pair, it reduces to a rotation at constant angular velocity $\omega_{\mathbf{n}}$ which is proportional to the wave number $k_{\mathbf{n}}$,

$$\omega_{\mathbf{n}} = v k_{\mathbf{n}},$$

where v has the dimension of a velocity.

In the remainder of the paper we state these results more precisely and give details about how they are obtained. They are of two types: First, a theoretical description of the modes, which is based on the symmetries of the system. Second, a detailed account of the numerical algorithms necessary to substantiate our claims (the difficulty being the decomposition of the $d^{(j)}$ dimensional spaces $M^{(j)}(\xi)$).

3. TANGENT-SPACE DYNAMICS

The dynamics of hard disks consists of phases of free flight interrupted by instantaneous elastic collisions. We denote the map for free flights of duration τ by F^τ, and the collision map by C. Then, the evolution of an initial state, ξ_0, is given by

$$\xi_t = F^{\tau_n} \circ \cdots \circ C \circ F^{\tau_2} \circ C \circ F^{\tau_1} \ \xi_0, \tag{3}$$

where $\tau_1, \ldots, \tau_n$ are the time intervals between successive collisions. The *tangent-space dynamics* of an infinitesimal perturbation $\delta\xi_0$ of ξ_0 is given by the tangent map of the flow (3):

$$\delta\xi_t = \mathrm{D}F^{\tau_n}\big|_{\xi_n^+} \cdots \mathrm{D}C|_{\xi_2^-} \cdot \mathrm{D}F^{\tau_2}\big|_{\xi_1^+} \cdot \mathrm{D}C|_{\xi_1^-} \cdot \mathrm{D}F^{\tau_1}\big|_{\xi_0} \ \delta\xi_0,$$

where ξ_k^- denotes the state just before the kth collision, and $\xi_k^+ = C(\xi_k^-)$ is the state immediately after.[9] Here, $\mathrm{D}F^\tau|_{\xi_k}$ and $\mathrm{D}C|_{\xi_k}$ are $4N \times 4N$ symplectic matrices. For the sake of simplicity, the flow is also called Φ^t: namely $\Phi^t(\xi_0) = \xi_t$, and we often write $\delta\xi_t = \mathrm{D}\Phi^t\big|_{\xi_0} \cdot \delta\xi_0$. By convention, if t is a collision time, $\delta\xi_t$ denotes a tangent vector immediately before that collision.

[9]We disregard problems of differentiability which appear for the (rare) tangent collisions.

3.1. Numerical Procedure and Lyapunov Modes

Extensive numerical simulations are used to establish the classification and dynamics of the modes. Here, we briefly summarize our algorithm described in detail in refs. 2,12 and provide a precise definition of the Lyapunov modes we observe. It is well known that the exponential growth rate of a typical k-dimensional volume element is given by $\lambda_1 + \cdots + \lambda_k$,

$$\lambda_1 + \cdots + \lambda_k = \lim_{t\to\infty} \frac{1}{t} \log \|\delta\xi_t^1 \wedge \cdots \wedge \delta\xi_t^k\|. \tag{4}$$

If the tangent vectors $\delta\xi^1, \ldots, \delta\xi^k$ are linearly independent at time zero, they will remain so, because the tangent flow is time reversible. Orthogonality is not preserved by the tangent flow, because, generally, $D\Phi^t$ is not an orthogonal matrix. However, (4) still holds if the vectors $\delta\xi_t^1, \ldots, \delta\xi_t^k$ are replaced by a (Gram-Schmidt) orthogonalized set of vectors $\delta\eta_t^1, \ldots, \delta\eta_t^k$.[10] It takes thus the simpler form

$$\lambda_1 + \cdots + \lambda_k = \lim_{t\to\infty} \frac{1}{t} \sum_{i=1}^{k} \log \|\delta\eta_t^i\|. \tag{5}$$

Since (5) holds for every $k \leqslant 4N$, the exponent λ_k turns out to be equal to the growth rate of the kth orthogonalized vector $\delta\eta_t^k$.

The numerical method of Benettin *et al.*[13] and Shimada *et al.*[14] – and indeed any algorithm – is based on this construction, although its basic objects are not the $\delta\eta_t^k$ vectors. As time increases, they all would get exponentially close to the most-unstable direction, become numerically indistinguishable, and diverge. Instead of orthogonalizing *once* at time t, the tangent dynamics is applied to a set of tangent vectors, which are periodically replaced by an orthogonalized set, that we denote by $\delta\gamma_t^1, \ldots, \delta\gamma_t^k$. The modified dynamics is therefore that of an orthogonal frame.[2,12] One assumes that (5) is still valid if $\delta\eta_t^k$ is replaced by $\delta\gamma_t^k$. The kth Lyapunov mode (or Lyapunov vector) at time t is, by definition, the vector $\delta\gamma_t^k$, and it is associated with the exponent λ_k.

Our study starts with the observation that we consider a system with non-trivial Lyapunov exponents. To guarantee the convergence of the numerical algorithm, additional properties of the dynamical system are needed: Namely, that the system has well-defined local stable and unstable subspaces associated with every Lyapunov exponent (close to zero).

[10] $\delta\eta_t^j = \delta\xi_t^j - \sum_{i=1}^{j-1} (\delta\xi_t^j \cdot \delta\xi_t^i)/(\|\delta\xi_t^i\|^2)\delta\xi_t^i$.

Results in this direction have been obtained for hard-disk systems in refs. 15–17. A stronger property, hyperbolicity, has been recently proved for hard disk systems with randomly chosen masses in refs. 18–20. We assume here that these results hold for our system as well. As already advocated in ref. 10, what matters from a physicist's point of view is that the numerical studies behave as if this were true. Under the above assumptions, the kth mode will align with the corresponding unstable subspace. In other words, measured modes will be orthogonal spanning sets of the $M^{(j)}$ subspaces defined in Eq. (1).

The algorithm we use in our numerical work[2,12] is based on the principles just outlined. We restrict our considerations to hard-disk systems without external interaction. Since there is no potential energy, the dynamics is the same at any (total) energy, up to a rescaling of time. The natural unit of time of the system is $((m\sigma^2 N)/K)^{1/2}$. Throughout, reduced units are used, for which the particle mass m, the disk diameter σ, and the kinetic energy per particle, K/N, are unity. The density, defined by $\rho = N/V$ and the aspect ratio, defined by $A = L_y/L_x$, are the only relevant macroscopic parameters. Here, $V = L_x L_y$ is the area of the (rectangular) simulation box whose sides are L_x and L_y in the x and y directions, respectively. All our numerical examples are for densities $\rho \leqslant 0.8$ characteristic of dense or dilute (if $\rho \leqslant 0.1$) hard disk gases. The results are insensitive to the time between successive Gram-Schmidt re-orthonormalization steps.

3.2. Modes and Oseledec Subspaces

We have remarked in Section 2 that the spaces $E^{(j)}$ of Oseledec' theorem are in general not identical to the spaces of the modes $M^{(j)}$ defined in the Eq. (1). Here, we explain this difference.

The covariant subspaces $E^{(1)}, \ldots, E^{(\ell)}$ of the Oseledec splitting are obtained as follows[10]: the multiplicative ergodic theorem (for reversible systems) states that the matrices

$$\Lambda_{\pm}(\xi) \equiv \lim_{t \to \pm\infty} (\mathrm{D}\Phi^{\pm t}\big|_{\xi}^{\mathrm{T}}\, \mathrm{D}\Phi^{\pm t}\big|_{\xi})^{\frac{1}{2|t|}}$$

exist with probability one. The eigenvalues of Λ_+ are $\exp(\lambda^{(1)}) > \cdots > \exp(\lambda^{(\ell)})$ and the eigenvalues of Λ_- are $\exp(-\lambda^{(\ell)}) > \cdots > \exp(-\lambda^{(1)})$. Since both Λ_+ and Λ_- are symmetric, their eigenspaces define two orthogonal decompositions of the tangent space

$$TX = U_{\pm}^{(1)} \oplus \cdots \oplus U_{\pm}^{(\ell)},$$

where $U_{\pm}^{(j)}$ is the eigenspace of $\Lambda_{\pm}$ associated to $\exp(\pm\lambda^{(j)})$. Note that the $U_{\pm}^{(j)}$ subspaces are pairwise orthogonal but in general *not* covariant. However, for $j \in \{1, \ldots, \ell\}$, the subspaces

$$U_{+}^{(j)} \oplus \cdots \oplus U_{+}^{(\ell)} \quad \text{and} \quad U_{-}^{(1)} \oplus \cdots \oplus U_{-}^{(j)}$$

are covariant. They are, respectively, the subspace of the $\ell - j + 1$ most stable directions of Λ_{+} and the subspace of the j most unstable directions of Λ_{-} (or equivalently its j most stable directions *in the past*). For every ξ, the invariant subspaces $E^{(j)}$ are then given by

$$E^{(j)} = \left(U_{-}^{(1)} \oplus \cdots \oplus U_{-}^{(j)}\right) \cap \left(U_{+}^{(j)} \oplus \cdots \oplus U_{+}^{(\ell)}\right).$$

The $E^{(j)}$ spaces are covariant but in general *not* orthogonal. One can show that

$$U_{-}^{(1)} \oplus \cdots \oplus U_{-}^{(j)} = E^{(1)} \oplus \cdots \oplus E^{(j)} \equiv F^{(j)},$$

where $F^{(j)}$ was introduced in Section 2. Using the definition (1), one easily verifies that $M^{(j)} = U_{-}^{(j)}$.

Remark 1. In our numerical method, the modes are obtained at the phase points $\Phi^t(\xi_0)$ for large t, *i.e.*, at the *end* of integrated trajectories. It is therefore consistent that they should contain information about the *past* and not the future, that is about Λ_{-} and not Λ_{+}.

In general, $U_{-}^{(j)}$, $U_{+}^{(j)}$ and $E^{(j)}$ are different. Hard-disk systems have a special property: the three spaces coincide for the Lyapunov exponent $\lambda^{(m)} = 0$, where $m \equiv \frac{1}{2}(\ell + 1)$ is the middle index. We shall denote by $\mathcal{N}$ the covariant subspace $\mathcal{N} = E^{(m)}$, also called the null subspace. In Section 4.1, we give the explicit form of $\mathcal{N}$. Using the explicit Jacobians for the particle collisions and for the free-streaming motion, as given in refs. 2, 12, 21 one can check that the orthogonal complement to the null subspace, $\mathcal{N}^{\perp}$, is also covariant. From this statement, one can show that $\mathcal{N} = U_{+}^{(m)} = U_{-}^{(m)}$. Our measured modes $M^{(m)} = U_{-}^{(m)}$ therefore span the null space. Since this argument seems to fail for $j \neq m$, we can only conclude that modes of $M^{(j)}$ are perturbations whose exponential growth rate is *at least* $\lambda^{(j)}$.

3.3. Two Simplifications

Two additional properties greatly simplify the classification of the modes: the symplecticity of the tangent flow and an observed property "δq is proportional to δp". The symplecticity of the tangent flow means that

$$D\Phi^t\big|_\xi^{\mathrm{T}}\, J\, D\Phi^t\big|_\xi = J, \tag{6}$$

where the $4N \times 4N$ matrix J is defined as[11]

$$J : \begin{pmatrix} \delta p \\ \delta q \end{pmatrix} \mapsto \begin{pmatrix} 0 & -1 \\ 1 & 0 \end{pmatrix} \begin{pmatrix} \delta p \\ \delta q \end{pmatrix} = \begin{pmatrix} -\delta q \\ \delta p \end{pmatrix}.$$

As a consequence of (6), both Λ_+ and Λ_- are symplectic (see *e.g.*, ref. 21) and, as is well known, Lyapunov exponents of Hamiltonian systems come in pairs $\lambda^{(j)}$, $\lambda^{(\ell-j+1)} = -\lambda^{(j)}$ of equal multiplicity. The matrix J relates the $U_\pm^{(j)}$ subspaces by

$$U_\pm^{(j)}(\xi) = J U_\pm^{(\ell-j+1)}(\xi). \tag{7}$$

Therefore, it is sufficient to measure the Lyapunov exponents and the modes for the positive part of the spectrum. Note that J is *not* the (derivative of the) velocity reversal $(\delta p, \delta q) \mapsto (-\delta p, \delta q)$ and does not change the sign of time.

The simulations of our system exhibit an additional structure which considerably simplifies the analysis of Lyapunov modes near zero. *Unstable* perturbations ($\lambda > 0$) have the (approximate) form

$$\delta p = C(\xi, \lambda)\delta q, \quad C > 0,$$

while the *stable* ($\lambda < 0$) perturbations are of the form

$$-C'(\xi, \lambda)\delta p = \delta q, \quad C' > 0.$$

Here, C and C' are *numbers*. In Figure 3 we demonstrate that the perturbations δq and δp associated with each Lyapunov mode are nearly parallel or anti-parallel for large N. Equation (7) also suggests $C = C'$, which is well verified by the simulations.

[11] With the reduced units defined above, positions and velocities are dimensionless.

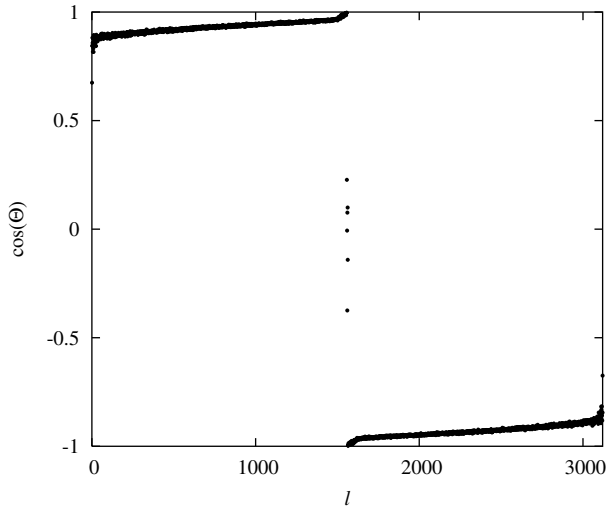

Fig. 3. Value of $\cos(\Theta) = (\delta q \cdot \delta p)/(|\delta q| \cdot |\delta p|)$, as a function of the Lyapunov index l for an instantaneous configuration of the system characterized in Fig. 1. Here, Θ is the angle between the $2N$-dimensional vectors of the perturbation components of all particle positions and velocities for a Lyapunov vector ξ_l. For the small positive exponents, for which $l < 2N - 2 = 1558$, this angle vanishes, for the small negative exponents, for which $l > 2N + 3 = 1563$, it is equal to π. For the six zero modes, $1558 \leqslant l \leqslant 1563$, the angle lies between these limiting values.

We can therefore restrict our classification to the δq part of the modes corresponding to positive exponents. If we can associate every measured exponent λ to a given δq, then we will know that the exponents λ and $-\lambda$ correspond to the modes $(\delta p, \delta q)$ with $\delta p = C\delta q$ and $\delta p = -C^{-1}\delta q$, respectively.

3.4. Tangent Vectors as Vector Fields

The components of a tangent vector $\delta\xi = (\delta p, \delta q)$ are the perturbation components of the positions and velocities of all particles. As a graphical representation of such a vector, we show in the left panel of Fig. 4 the instantaneous positional perturbations of all particles *at their positions* in physical space, where the arrows indicate the directions and strengths. It belongs to a Lyapunov exponent λ_{1546} indicated by the enlarged circle in Fig. 5. A qualitatively identical figure is obtained, if the positional displacements of all particles are replaced by their momentum displacements, as explained in Section 3.3. Thus, this figure is a complete representation

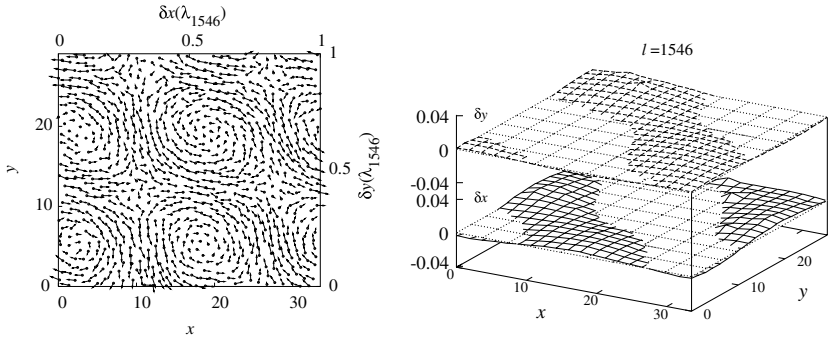

Fig. 4. The transverse mode T(1,1) for λ_{1546} of Fig. 5. Left: Interpretation as a vector field; Right: Alternative representation as periodic spatial patterns of the position perturbations δx_i and δy_i of the particles, which emphasizes the wave vector parallel to a diagonal of the simulation box.

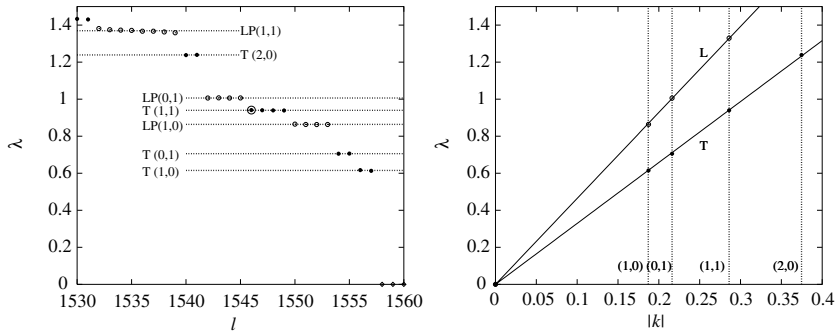

Fig. 5. Lyapunov spectrum and "dispersion relations" for the 780-disk system characterized in Fig. 1, and the density $\rho = 0.8$. Left: Lyapunov exponents are ordered by size and repeated with multiplicities. The specially marked point corresponds to the transverse mode shown in Fig. 4. Right: Lyapunov exponents as a function of their wave number. The respective labels L and T refer to the longitudinal and transverse branches.

of the Lyapunov vector $\delta\xi = (\delta p, \delta q)$ belonging to λ_{1546} in Fig. 5. The transverse modes for λ_{1549} on the left panel of Fig. 2, and for λ_{1548} at the bottom left panel of Fig. 6, are other examples of transverse modes belonging to the same degenerate exponent.

We interpret the left panel of Fig. 4 as a two-dimensional *vector field* φ which – up to a constant phase – is well described by

$$\begin{pmatrix}\varphi_x(x,y)\\ \varphi_y(x,y)\end{pmatrix} = \begin{pmatrix}\alpha_1 \cos(k_x x)\sin(k_y y)\\ -\alpha_2 \sin(k_x x)\cos(k_y y)\end{pmatrix},$$

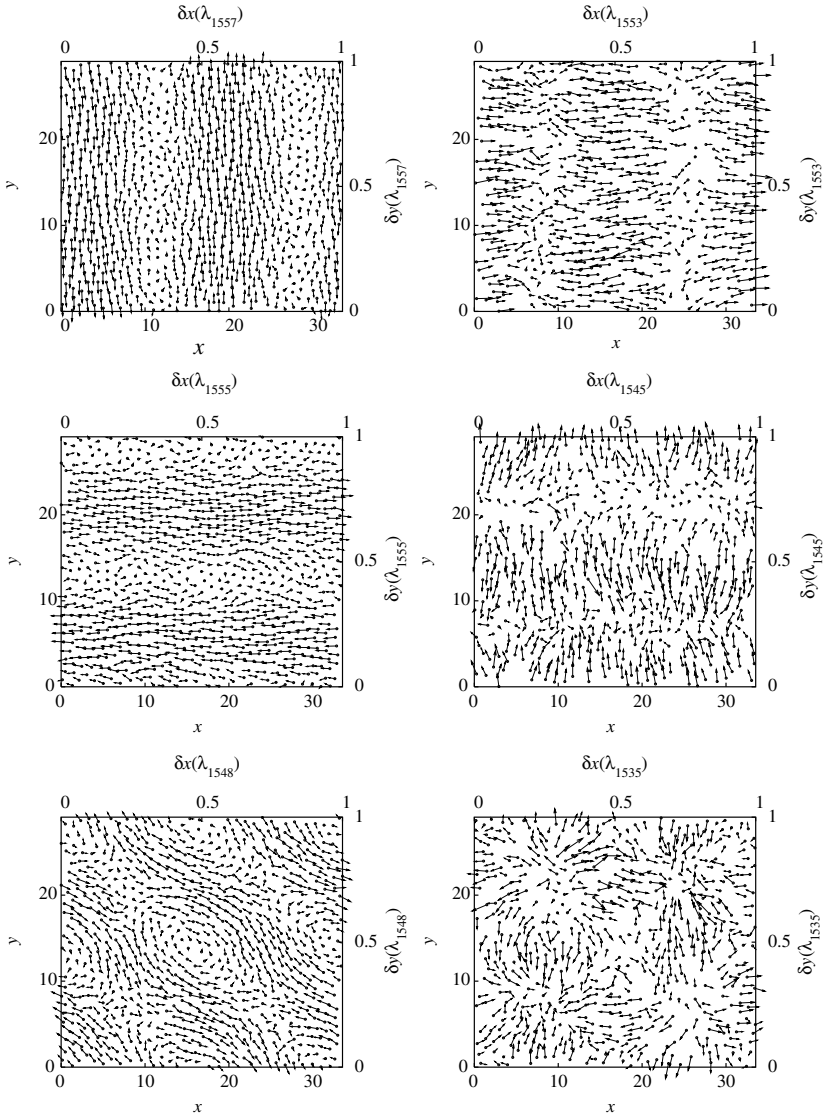

Fig. 6. Snapshots of Lyapunov modes for the periodic 780-disk system of Section 4. Left, from top to bottom: Transverse modes T(1,0), T(0,1), and T(1,1) belonging to $\lambda_{1557}, \lambda_{1555}$, and λ_{1548}, respectively, of Fig. 5. Right, from top to bottom: Vector fields for longitudinal modes, which belong to the LP pairs LP(1,0), LP(0,1), and LP(1,1), and which are associated with the respective exponents $\lambda_{1553}, \lambda_{1545}$ and λ_{1535}, of Fig. 5.

where $k_x = \frac{2\pi}{L_x}$ and $k_y = \frac{2\pi}{L_y}$, and α_1, α_2 are two constants. For this reason, we assign the node numbers $(n_x, n_y) = (1, 1)$ to this mode.

To be more precise, let $r = (x, y) \in [0, L_x) \times [0, L_y)$. We say that a two-dimensional smooth vector field $\varphi = (\varphi_x, \varphi_y)$ over the position space, is *sampled* by the infinitesimal displacements δq of the N disks at their reference positions q, when

$$\varphi(q_j) = \delta q_j, \quad \text{for all } j = 1, \ldots, N.$$

Thinking of a tangent vector in terms of an associated vector field is meaningful if there are "sufficiently" many particles to sample the field on a typical length scale of its variation. Once this condition breaks down for larger exponents, as it will for large-enough k, the modes disappear[12], and so do the steps in the Lyapunov spectrum. In the following we use a notation which does not distinguish between tangent vectors and their two-dimensional vector fields.

4. OBSERVATION AND DESCRIPTION OF THE MODES

In this section, we describe the Lyapunov spectrum near 0 and the corresponding modes, as they are measured in numerical experiments. In the two following subsections, we will explain how these modes can be understood on the basis of symmetry breaking of "zero modes".

We illustrate our assertions with the system already introduced in Fig. 1, which contains $N = 780$ particles in a rectangular periodic box with an aspect ratio $L_y/L_x = 0.867$. It corresponds to a hard-disk gas with a density $\rho = 0.8$, slightly below the fluid-to-solid phase transition density.[12] The left panel of Fig. 5 provides a magnified view of the smallest positive Lyapunov exponents for this system.[13] The exponents, ordered by size and repeated with their multiplicities, are plotted as a function of their index. Degenerate exponents with a multiplicity $d \geqslant 2$ appear therefore as "steps". To account for the wave-like appearance of the modes, we associate with each Lyapunov vector a wave number $k_{(n_x, n_y)}$, as in (2), where the non-negative integers $\mathbf{n} = (n_x, n_y)$ count the nodes in the respective directions.[14]

When the small Lyapunov exponents are plotted as a function of their corresponding wave number, they all lie on two curves, sometimes referred

[12] And the sampled vector field is ill-defined.

[13] The conjugate negative exponents are not shown, see refs. 2, 8.

[14] In many cases, the number of nodes is easy to determine, as in Fig. 4. To facilitate an objective identification of the wave vectors modes associated with larger exponents, which are noisier, Fourier-transforms are used.

Table I. Central Subspace for the Vanishing Lyapunov Exponents. Notation: 1 = (1, 1, . . . , 1), and 0 = (0, 0, . . . , 0). All vectors have $4N$ components

Transformation	Generator
$(p, q) \mapsto (p_x + \varepsilon 1, p_y, q_x, q_y)$	$\delta\xi_1 = (1, 0, 0, 0)$
$(p, q) \mapsto (p_x, p_y + \varepsilon 1, q_x, q_y)$	$\delta\xi_2 = (0, 1, 0, 0)$
$(p, q) \mapsto (p_x, p_y, q_x + \varepsilon 1, q_y)$	$\delta\xi_3 = (0, 0, 1, 0)$
$(p, q) \mapsto (p_x, p_y, q_x, q_y + \varepsilon 1)$	$\delta\xi_4 = (0, 0, 0, 1)$
$(p, q) \mapsto (p_x + \varepsilon p_x, p_y + \varepsilon p_y, q_x, q_y)$	$\delta\xi_5 = (p_x, p_y, 0, 0)$
$(p, q) \mapsto (p_x, p_y, q_x + \varepsilon p_x, q_y + \varepsilon p_y)$	$\delta\xi_6 = (0, 0, p_x, p_y)$

to as "dispersion relations".[2,8] This is demonstrated on the right panel of Fig. 5. On this plot, degenerate exponents are represented by a single point. For reasons discussed below, the upper branch is called *longitudinal* (L), and the lower *transverse* (T). It is experimentally found that for a given wave number, the multiplicity of the L branch is twice that of the T branch, as mentioned already in Section 2.

4.1. Vanishing Lyapunov Exponents

We start our description with the six modes associated with the six vanishing Lyapunov exponents, commonly referred to as *zero modes*. Four of them are induced by the homogeneity of space, and two are consequences of the homogeneity of time. They span a six-dimensional subspace $\mathcal{N}(\xi)$ of the tangent space, $TX(\xi)$, at any phase point ξ.[15] These 6 zero modes play a fundamental role in understanding the nature of the modes associated with Lyapunov exponents close to zero.

In order to show which symmetries give rise to the zero modes, we list in Table I the six corresponding elementary transformations. This defines the six zero modes $\delta\xi_1$ to $\delta\xi_6$ in a notation that separates the x and y components of δp and δq. The vectors $\delta\xi_1$ and $\delta\xi_2$ correspond to a perturbation of the total momentum in the x and y directions, $\delta\xi_3$ and $\delta\xi_4$ to an (infinitesimal) uniform translation of the origin, $\delta\xi_5$ to a change of energy, and $\delta\xi_6$ to a change of the origin of time.

One can explicitly check that the subspace $\mathrm{Span}\{\delta\xi_1, \ldots, \delta\xi_6\}$ is covariant and that its vectors have a sub-exponential growth (or decay). It thus coincides with the null space $\mathcal{N}(\xi)$ of Section 3.2.

Remark 2. The space $\mathcal{N}(\xi)$ can be further decomposed into three covariant subspaces $\mathcal{N}_x = \mathrm{Span}\{\delta\xi_1, \delta\xi_3\}$, $\mathcal{N}_y = \mathrm{Span}\{\delta\xi_2, \delta\xi_4\}$ and $\mathcal{N}_p =$

[15] It is important to keep in mind that $\mathcal{N}(\xi)$ really depends on ξ, see below.

Span$\{\delta\xi_5, \delta\xi_6\}$, each of which independently satisfies the properties listed for $\mathcal{N}(\xi)$. In systems with reflecting boundaries, only $\mathcal{N}_p$ is present, while $\mathcal{N}_x$ and $\mathcal{N}_y$ are absent, because they are related to translation invariance. If only the x direction is periodic,[6] the space of zero modes is reduced to $\mathcal{N}_x \oplus \mathcal{N}_p$.

4.2. Longitudinal, Transverse and P-Modes

Following our argument of Section 3.3, we need only describe the δq part of the modes. Therefore, we consider the three transformations (see Table I)

$$\begin{aligned} \delta\xi_3 &: (q_{x,j}, q_{y,j}) \mapsto (q_{x,j} + \varepsilon, q_{y,j}) \\ \delta\xi_4 &: (q_{x,j}, q_{y,j}) \mapsto (q_{x,j}, q_{y,j} + \varepsilon) \\ \delta\xi_6 &: (q_{x,j}, q_{y,j}) \mapsto (q_{x,j} + \varepsilon p_{x,j}, q_{y,j} + \varepsilon p_{y,j}), \end{aligned} \tag{8}$$

associated to zero modes, and claim the following:

Modes Classification I: Modes of wave number $k_{\mathbf{n}}$ are scalar modulations of (8) with wave number $k_{\mathbf{n}}$. More precisely, they are obtained by replacing ε with $\varepsilon A(q_{x,j}, q_{y,j})$ in (8), where the real scalar function A is of the form

$$A(x, y) = \sum_{|\ell|=n_x, |m|=n_y} c_{\ell,m} \exp\bigl(i(\ell k_x x + m k_y y)\bigr).$$

The space of such modulations has dimension 4 in general and dimension 2 if either n_x or n_y vanishes.

Example 1. We consider $\mathbf{n} = (1, 0)$, $(0, 1)$ and $(1, 1)$. We use the notation $c_x = \cos(k_x x)$, $s_x = \sin(k_x x)$, $c_y = \cos(k_y y)$ and $s_y = \sin(k_y y)$. A basis of the space of functions with wave number $k_{\mathbf{n}}$ is shown in Table II. Of course, this choice fixes a constant phase for the sine and cosine functions.

Table II. Functions with Wave Number $k_{\mathbf{n}}$

$\mathbf{n}$	Function A	dim
(1,0)	c_x, s_x	2
(0,1)	c_y, s_y	2
(1,1)	$c_x c_y, s_x c_y, c_x s_y, s_x s_y$	4

If the Lyapunov exponent were a function of $k_{\mathbf{n}}$ only, we would expect 12-fold degeneracy in Fig. 5, (resp. 6-fold if either n_x or $n_y = 0$), since each of the three perturbations of (8) can be modulated by the four (resp. two) functions of Table II. However, this degeneracy is broken into an $8+4$ (resp. $4+2$) structure:

Mode Classification II: The Lyapunov vectors of wave number $k_{\mathbf{n}}$ have two possible Lyapunov exponents: $|\lambda| = c_{\mathrm{T}}|k_{\mathbf{n}}|$ or $|\lambda| = c_{\mathrm{L}}|k_{\mathbf{n}}|$, corresponding to the Transverse or Longitudinal branch of Fig. 5. The modes for these two branches are obtained as follows:

(1) Transverse branch: transverse modes are obtained by combining the modulations of $\delta\xi_3$ and $\delta\xi_4$ in a *divergence-free* vector field. We denote by $\mathrm{T}(\mathbf{n})$ the space of such vector fields.

(2) Longitudinal branch:

(i) Longitudinal modes are *irrotational* vector fields one obtains by combining the modulations of $\delta\xi_3$ and $\delta\xi_4$. We denote the corresponding space by $\mathrm{L}(\mathbf{n})$.

(ii) P-modes are modulations of $\delta\xi_6$, and we denote the corresponding subspace by $\mathrm{P}(\mathbf{n})$.

The three subspaces $\mathrm{T}(\mathbf{n})$, $\mathrm{L}(\mathbf{n})$ and $\mathrm{P}(\mathbf{n})$ have dimension 4 (or dimension 2 if either n_x or n_y vanishes). We denote by $\mathrm{LP}(\mathbf{n}) \equiv \mathrm{L}(\mathbf{n}) \oplus \mathrm{P}(\mathbf{n})$ the subspace corresponding to the Longitudinal branch. It has dimension 8 (4 if either n_x or n_y vanishes).

Remark 3. The divergence and curl of a vector field $\varphi = (\varphi_x, \varphi_y)$ are, of course,

$$\nabla \cdot \varphi = \partial_x \varphi_x + \partial_y \varphi_y, \quad \nabla \wedge \varphi = \partial_x \varphi_y - \partial_y \varphi_x.$$

Since every two-dimensional vector field uniquely decomposes into a sum of a divergence-free and an irrotational vector field, the spaces $\mathrm{L}(\mathbf{n})$ and $\mathrm{T}(\mathbf{n})$ span all possible two-dimensional vector fields of wave number $k_{\mathbf{n}}$.

There is a simple way to build $\mathrm{P}(\mathbf{n})$, $\mathrm{L}(\mathbf{n})$ and $\mathrm{T}(\mathbf{n})$ from the scalar modulations of Table II. If A is a modulation of wave number $k_{\mathbf{n}}$, then we have

$$pA \in \mathrm{P}(\mathbf{n}), \quad \nabla A \in \mathrm{L}(\mathbf{n}), \quad \nabla \wedge A \in \mathrm{T}(\mathbf{n}), \tag{9}$$

where by definition

$$\nabla A = \begin{pmatrix} \partial_x A \\ \partial_y A \end{pmatrix}, \quad \nabla \wedge A = \begin{pmatrix} \partial_y A \\ -\partial_x A \end{pmatrix}.$$

This construction is also useful because it naturally defines what we shall call *LP pairs*, by which we denote a field of L(**n**) and a field of P(**n**) originating from the same scalar modulation, as in (9). We show below that LP pairs play an important role. Indeed, when only some of the modes are present because of the boundary conditions, LP pairs are never broken: both fields are present, or both are missing (see Section 4.3). We shall also see in Section 5 that the dynamics of the modes mostly takes place between LP pairs.

Example 2. For the three modes of lowest wave number, Table III lists a basis of T(**n**), L(**n**) and P(**n**). Fields are given in a non-normalized form to keep notation short. Corresponding L(**n**) fields and P(**n**) fields are LP pairs. Figure 6 provides examples for T- and L-modes.

Modes of L(**n**) and T(**n**) are wavelike perturbations of the position space, and, therefore, are similar to the modes that appear in hydrodynamics (see Section 7). In particular, when either n_x or n_y vanish, the fields of L(**n**) and T(**n**) are, respectively, longitudinal and transverse to the wave vector. This observation is the reason for the names of the two branches in Fig. 5. To stay in line with this now-accepted terminology, we keep it also for the case $n_x \cdot n_y \neq 0$. P-modes are more complex than the other modes, because they depend not only on the positions of the perturbed particles but also on their velocities.

Table III. Decomposition of n-Modes for Rectangular Systems with Periodic Boundaries

n	Basis of T(**n**)	Basis of L(**n**)	Basis of P(**n**)
(1,0)	$\begin{pmatrix} 0 \\ c_x \end{pmatrix}, \begin{pmatrix} 0 \\ s_x \end{pmatrix}$	$\begin{pmatrix} c_x \\ 0 \end{pmatrix}, \begin{pmatrix} s_x \\ 0 \end{pmatrix}$	$\begin{pmatrix} p_x \\ p_y \end{pmatrix} s_x, \begin{pmatrix} p_x \\ p_y \end{pmatrix} c_x$
(0,1)	$\begin{pmatrix} c_y \\ 0 \end{pmatrix}, \begin{pmatrix} s_y \\ 0 \end{pmatrix}$	$\begin{pmatrix} 0 \\ c_y \end{pmatrix}, \begin{pmatrix} 0 \\ s_y \end{pmatrix}$	$\begin{pmatrix} p_x \\ p_y \end{pmatrix} s_y, \begin{pmatrix} p_x \\ p_y \end{pmatrix} c_y$
(1,1)	$\begin{pmatrix} \frac{1}{k_x} c_x s_y \\ -\frac{1}{k_y} s_x c_y \end{pmatrix}, \begin{pmatrix} \frac{1}{k_x} s_x c_y \\ -\frac{1}{k_y} c_x s_y \end{pmatrix}$ $\begin{pmatrix} \frac{1}{k_x} s_x s_y \\ \frac{1}{k_y} c_x c_y \end{pmatrix}, \begin{pmatrix} \frac{1}{k_x} c_x c_y \\ \frac{1}{k_y} s_x s_y \end{pmatrix}$	$\begin{pmatrix} \frac{1}{k_y} c_x s_y \\ \frac{1}{k_x} s_x c_y \end{pmatrix}, \begin{pmatrix} \frac{1}{k_y} s_x c_y \\ \frac{1}{k_x} c_x s_y \end{pmatrix}$ $\begin{pmatrix} \frac{1}{k_y} s_x s_y \\ -\frac{1}{k_x} c_x c_y \end{pmatrix}, \begin{pmatrix} \frac{1}{k_y} c_x c_y \\ -\frac{1}{k_x} s_x s_y \end{pmatrix}$	$\begin{pmatrix} p_x \\ p_y \end{pmatrix} s_x s_y, \begin{pmatrix} p_x \\ p_y \end{pmatrix} c_x c_y$ $\begin{pmatrix} p_x \\ p_y \end{pmatrix} c_x s_y, \begin{pmatrix} p_x \\ p_y \end{pmatrix} s_x c_y$

At this point we are able to characterize the spectrum and its multiplicities with only two constants, c_L and c_T, which have the physical dimension of *velocities*. We shall see in Section 6 that these velocities depend on the density of the system, but are insensitive to the system size, the boundary type, and the aspect ratio. Therefore, it is tempting to think of c_L and c_T as thermodynamic velocities. However, as discussed in Section 6, no obvious interpretation could be found so far.

4.3. Other Aspect Ratios and Boundary Conditions

We summarize here some observations which concern different boundary conditions and degeneracies.

(i) The Lyapunov spectrum is more degenerate for square systems, for which $k_{(n_x,n_y)} = k_{(n_y,n_x)}$. In this case the multiplicities are doubled with respect to the general case, for which $n_x \neq n_y$. Other "accidental" degeneracies may occur: for instance, parameters can be found for which $c_T|k_{(1,1)}| = c_L|k_{(1,0)}|$.

(ii) Systems with *reflecting* boundaries[6] develop only a subset of the modes encountered so far, which can be found by the following simple, and obvious, rules:

- The fundamental wave vectors are $k_x = \frac{\pi}{L_x}$ and $k_y = \frac{\pi}{L_y}$ (not 2π). Here, L_x and L_y are the *effective* box sizes, obtained from the actual side lengths by subtracting one particle diameter σ.
- The fields of $T(\mathbf{n})$ and $L(\mathbf{n})$ have to satisfy Dirichlet conditions, namely to be tangent to the boundary:

$$\varphi_x(0, y) = \varphi_x(L_x, y) = 0 \quad \text{and} \quad \varphi_y(x, 0) = \varphi_y(x, L_y) = 0.$$

If expressed in terms of sines and cosines, this means that φ_x may contain $\sin(k_x x)$ but not $\cos(k_x x)$, and so on.

- As for periodic boundary conditions, when an L-mode is present, its paired P-mode is always present.

(iii) Hybrid systems with reflecting boundaries in one direction and periodic boundaries along the other behave as expected:[6] the fundamental wave vectors are chosen according to the boundary type, and the Dirichlet conditions are only applied to one component of the field.

Table IV. Mode Decomposition for Rectangular Systems with Reflecting Boundaries

n	T(**n**)	L(**n**)	P(**n**)
(1,0)	none	$\begin{pmatrix} s_x \\ 0 \end{pmatrix}$	$\begin{pmatrix} p_x \\ p_y \end{pmatrix} c_x$
(0,1)	none	$\begin{pmatrix} 0 \\ s_y \end{pmatrix}$	$\begin{pmatrix} p_x \\ p_y \end{pmatrix} c_y$
(1,1)	$\begin{pmatrix} s_x c_y \\ -c_x s_y \end{pmatrix}$	$\begin{pmatrix} s_x c_y \\ c_x s_y \end{pmatrix}$	$\begin{pmatrix} p_x \\ p_y \end{pmatrix} c_x c_y$

(iv) Narrow systems, for instance those with $\sigma < L_y < 2\sigma$ and $L_x \gg \sigma$,[16] only develop modes with $n_y = 0$.[23] This follows, since a vector field varying along the y axis cannot be sampled by a single particle. Therefore, the Lyapunov spectrum of such a system is greatly simplified, since the modes are restricted to $\mathrm{L}(n_x, 0)$ and $\mathrm{T}(n_x, 0)$.

Example 3. Table IV shows which modes of Table III satisfy the Dirichlet condition and are thus present in a system with reflecting boundaries.[17] We stress that such a system has only *two* vanishing Lyapunov exponents which are associated with $\delta\xi_5$ and $\delta\xi_6$ of Table I. *Therefore, modes appear which are not modulations of zero modes of the system.* The crucial observation here is that even if one of the fundamental symmetries is broken by the boundary condition, the modulation, as defined in Eq. (9), may still satisfy that boundary condition. For example, if we have reflecting boundaries on the walls $\{x = 0\}$ and $\{x = L_x\}$, then any perturbation $A(x, y) = \sin(mk_x x)B(y)$ will be acceptable, whereas, of course, $A(x, y) = \cos(mk_x x)B(y)$ would not.

Systems with reflecting boundaries and narrow systems are easier to study numerically, because the multiplicities of the L, P and T spaces are smaller than in the periodic rectangular case. In particular, the LP(1,1) space has only dimension 2 when the boundaries are reflecting. For that reason, we illustrate some of the issues below also with the "reflecting-wall version" of the 780-disk system introduced in Fig. 8.

[16] Recall that σ is the diameter of the disks.

[17] For such a choice of basis vectors the origin of the coordinate system is at the bottom-left corner of the simulation box.

4.4. How to Measure P-Modes

Contrary to L(**n**) and T(**n**), the tangent subspace P(**n**) *depends on the state that it perturbs*. Moreover, modes of P(**n**) are not really vector fields, because the velocities of the particles in a typical configuration do not depend smoothly on position. In order to "see" a P-mode, we face two problems:

(i) A typical measured vector of an LP(**n**) space is a *superposition* of vectors of L(**n**) and P(**n**).

(ii) Even when a mode of P(**n**) is isolated, it is not smooth and does not "look like" a vector field over the box.

We explain our solution to the first problem with the simplest possible example: the LP(1, 0) space for a rectangular system with *reflecting boundaries* (see Section 4.3). This space has dimension two and is defined by the two normalized spanning vectors

$$\begin{pmatrix}\varphi_x^{\mathrm{L}}\\ \varphi_y^{\mathrm{L}}\end{pmatrix}=\frac{1}{z_1}\begin{pmatrix}s_x\\ 0\end{pmatrix},\quad \begin{pmatrix}\varphi_x^{\mathrm{P}}\\ \varphi_y^{\mathrm{P}}\end{pmatrix}=\frac{1}{z_2}\begin{pmatrix}p_x\\ p_y\end{pmatrix}c_x,\quad k_x=\frac{\pi}{L_x}, \tag{10}$$

where z_1 and z_2 are normalization constants. At any time t, we have two measured modes, ψ^1 and ψ^2 (vectors with $2N$ components, since only the δq part is observed), whose span is (numerically very close to) LP(1, 0). Therefore, there are constants a, b, c, d with

$$\begin{aligned}\varphi^{\mathrm{L}} &= \psi^1 a+\psi^2 b,\\ \varphi^{\mathrm{P}} &= \psi^1 c+\psi^2 d.\end{aligned} \tag{11}$$

Since all these vectors are normalized, one should also have $a^2+b^2=c^2+d^2=1$. However, Eq. (11) is over-determined: four constants have to satisfy $4N$ equations. Numerically, we use a least-square method to find the best values for a, b, c and d, which we denote by α, β, γ, δ.[18] Thus, the measured modes, ψ^1 and ψ^2, are decomposed according to

$$\begin{aligned}\tilde{\varphi}^{\mathrm{L}} &= \psi^1\alpha+\psi^2\beta,\\ \tilde{\varphi}^{\mathrm{P}} &= \psi^1\gamma+\psi^2\delta,\end{aligned}$$

[18] It is also possible to use a simple projection $\alpha=\varphi^{\mathrm{L}}\cdot\psi^1$, etc. This method assumes that φ^{L} and φ^{P} are orthogonal vectors, which they only are approximately.

where the vectors $\tilde{\varphi}^{\mathrm{L}}$ and $\tilde{\varphi}^{\mathrm{P}}$ are the best-possible LP-pair, φ^{L} and φ^{P}, reconstructed from experimental data.

Now we can deal with our second problem: whereas the vector $\tilde{\varphi}^{\mathrm{L}}$ is easily recognized as a vector field, the vector $\tilde{\varphi}^{\mathrm{P}}$ is not. However, from (10) we deduce that

$$\begin{pmatrix} \varphi_x^{\mathrm{P}}/p_x \\ \varphi_y^{\mathrm{P}}/p_y \end{pmatrix} = \begin{pmatrix} c_x \\ c_x \end{pmatrix},$$

or, more precisely,

$$\begin{pmatrix} \varphi_{x,j}^{\mathrm{P}}/p_{x,j} \\ \varphi_{y,j}^{\mathrm{P}}/p_{y,j} \end{pmatrix} = \begin{pmatrix} \cos(k_x q_{x,j}) \\ \cos(k_x q_{x,j}) \end{pmatrix}, \quad j = 1, \ldots, N. \tag{12}$$

Therefore, both $\varphi_x^{\mathrm{P}}/p_x$ and $\varphi_y^{\mathrm{P}}/p_y$ are smooth functions and can be easily visualized.

Remark. (i) This procedure readily extends to higher-dimensional LP(**n**) spaces, for instance to the four-dimensional LP(1, 1) space of a periodic system. We take this case as an example to illustrate in Fig. 7 our method of mode reconstruction: from the four measured modes the analogue to Eq. (11) generates four spanning vectors, namely two L-modes (one of which is shown at the top-right position of Fig. 4) and two P-modes. The x and y components of one of the P-modes, namely $\tilde{\varphi}^{\mathrm{P}} \approx ps_x$, are shown in the top row of Fig. 7. No smooth functions are recognized. However, after dividing by the momentum components, $p_{x,j}$ and $p_{y,j}$, as required by (12), the figures for the fields $\tilde{\varphi}_x^{\mathrm{P}}/p_x$ and $\tilde{\varphi}_y^{\mathrm{P}}/p_y$ in the bottom row of Fig. 7 clearly display the expected s_x-dependence.

(ii) Division by $p_{x,j}$ or $p_{y,j}$ in (12) is numerically unstable when particle j has a very small momentum along a coordinate axis. We avoid this by multiplying instead by $p_{x,j}/(p_{x,j}^2 + \varepsilon)$, where $\varepsilon \ll 1$. One could also ignore particle j in this case and only sample the field at those points where both $p_{x,j}$ and $p_{y,j}$ are not too small.

5. DYNAMICS OF THE MODES

Remark. The interested reader can look up animated pictures on the web at the address http://theory.physics.unige.ch/modes/.

In this section we turn to the "dynamics of the modes" and study what has been called the velocity of the longitudinal modes.[2,5,7] This might clarify hydrodynamic theories,[4,5] which are mostly based on a partial classification of the modes. In numerical simulations, the *transverse*

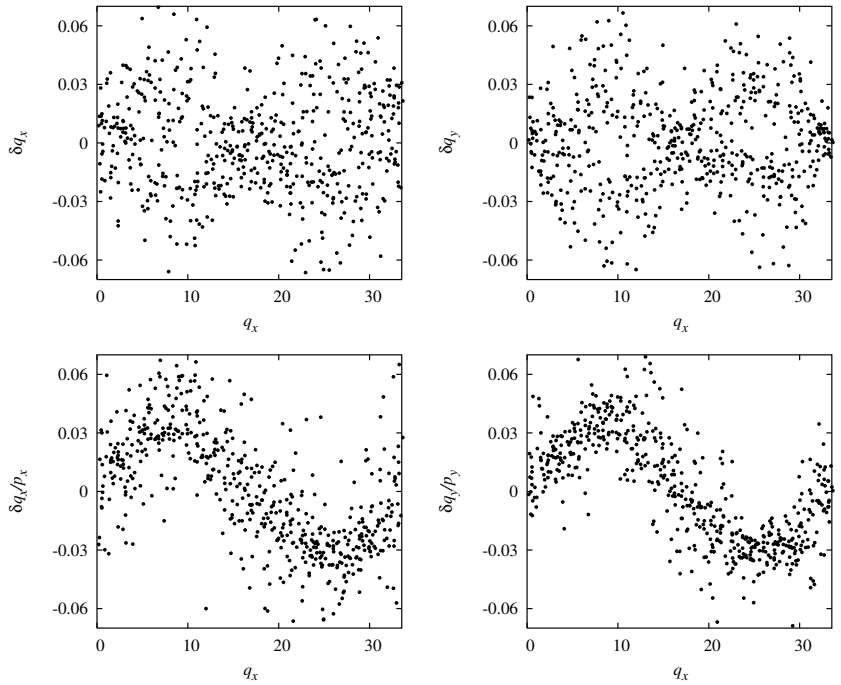

Fig. 7. Example for the P-mode reconstruction for the four-dimensional LP(1,0) space of a system with *periodic boundaries*. Only half of the components are shown, namely those corresponding to s_x. The c_x components are similar. Top row: x and y components of the reconstructed P-mode $\tilde{\varphi}^{\mathrm{P}} \approx p s_x$. Bottom row: the fields $\tilde{\varphi}_x^{\mathrm{P}}/p_x$ and $\tilde{\varphi}_y^{\mathrm{P}}/p_y$ are wavelike again. Note that in the top row one can recognize the sinusoidal envelope.

modes are stationary in space and time: although the particles move, the vector-field of the mode does not. In other words, at any instant of time, the vector field of a T-mode does not move (up to a small jitter due to numerical noise).

For *longitudinal* modes, however, one seems to observe[24] a propagation in the direction of the wave vector.[19] Using the geometrical picture developed above, we can interpret this motion and also explain why no propagation is observed for the LP dynamics in systems with reflecting boundaries as demonstrated in Fig. 8 below.

Since multiplicities are not so essential here, we illustrate the interpretation for the (simpler) LP(1, 1) space of a rectangular system with reflecting boundaries (dimension 2). In Section 4.4 we pointed out that at any

[19] When either n_x or n_y vanish, for instance in the L(1, 0) or L(0, 1) space.

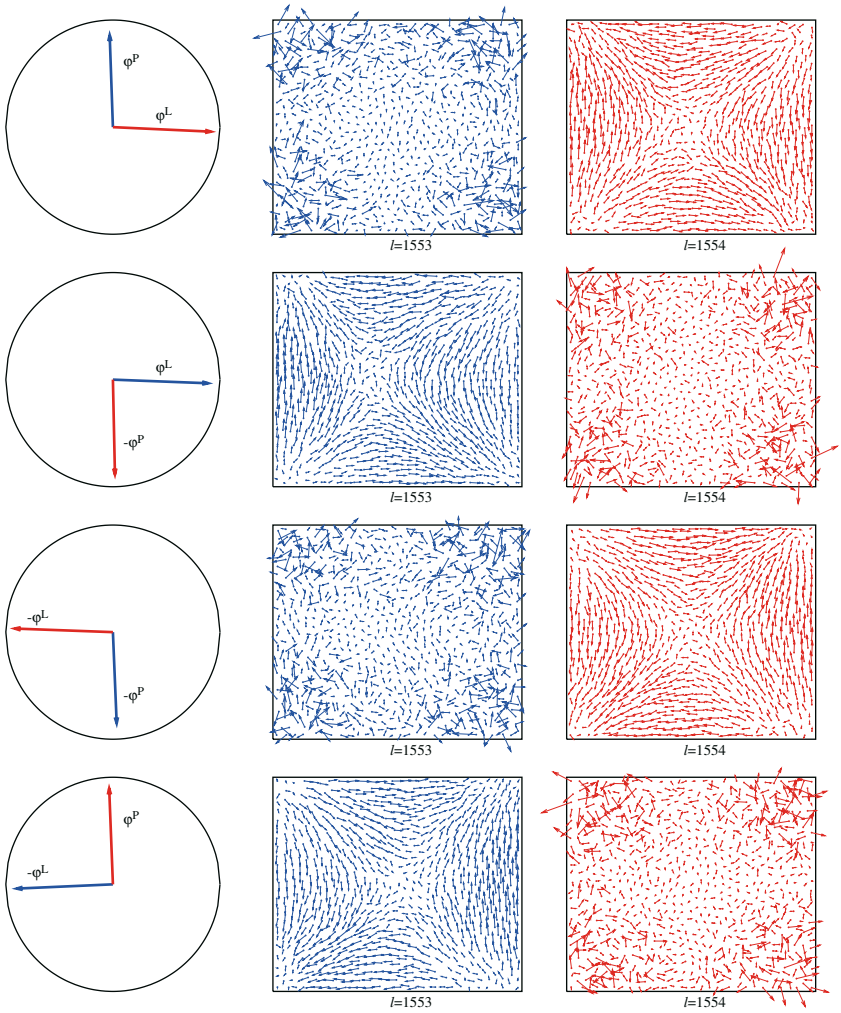

Fig. 8. LP(1,1) dynamics for a system of 780 disks in a box with an aspect ratio 0.867, a density 0.8, and with *reflecting* boundaries. Left: coordinates of the measured fields in the "standard basis" of LP(1,1). The (unit) circle is nearly reached, showing that indeed ψ^1 and ψ^2 span the same subspace as φ^{L} and φ^{P}. Center and right: the measured fields $\psi^1(t)$ and $\psi^2(t)$. The rows from top to bottom are consecutive snapshots separated by time steps of $\Delta t = 3.20$, which corresponds to a phase shift of $\pi/2$ in the LP(1,1) rotation. (A color figure is available online.)

given time t, where the state is ξ_t, the measured modes $\psi^1(t)$ and $\psi^2(t)$ are combinations of the two spanning vectors $\varphi^{\mathrm{L}}(\xi_t)$ and $\varphi^{\mathrm{P}}(\xi_t)$. We rewrite Eq. (11) in matrix form, but now with explicit time dependence:

$$\left(\varphi^{\mathrm{L}}(\xi_t), \varphi^{\mathrm{P}}(\xi_t)\right) = \left(\psi^1(t), \psi^2(t)\right) \cdot Q(t), \quad Q(t) = \begin{pmatrix} a(t) & b(t) \\ c(t) & d(t) \end{pmatrix}.$$

Therefore, the dynamics of the modes reduces to that of the 2×2 matrix $Q(t)$. In our simulations we keep the spanning vectors orthonormal. Since (in the experiment) the two fields φ^{L} and φ^{P} are also (nearly) orthogonal[20], the matrix $Q(t)$ is close to a *rotation* matrix (that is $c \simeq -b$, $d \simeq a$, and $a^2 + b^2 \simeq 1$). Therefore, the dynamics in the two-dimensional subspace is well described by a phase $\phi(t) = \arctan(b(t)/a(t))$.

LP-dynamics in 2 dimensions: The matrix $Q(t)$ is a rotation with constant angular velocity $\omega_{\mathbf{n}}$. This velocity is proportional to the wave number $k_{\mathbf{n}}$, namely

$$\phi(t) = \omega_{\mathbf{n}} t = v k_{\mathbf{n}} t.$$

Here, v is the product of a frequency and a wavelength and, therefore, is a *velocity*. According to the simulations, v depends only on the density of the system.

Example 4. In Fig. 8 we demonstrate this rotation in the LP(1,1) space of a system with reflecting boundaries. Snapshots of the two measured fields at consecutive times show the rotation of the two vectors between the L and the P direction.

A similar rotation has been found in narrow systems in ref. 6 and explained in refs. 5, 7 in the low density limit using a Boltzmann-equation approach.

Remark 4. The velocity $v = \omega_{\mathbf{n}}/|k_{\mathbf{n}}|$ has been interpreted earlier[24] as the phase velocity of a traveling wave in physical space. In Appendix A we demonstrate how the two interpretations can be reconciled. The definitions given above allow us to apply the same concepts also to the LP-dynamics of systems with reflecting boundaries, although they do not show traveling but standing waves.

[20] The scalar product $\varphi^{\mathrm{L}} \cdot \varphi^{\mathrm{P}} = \Sigma_{j=1}^{N} \cos(k_x q_{j,x}) \sin(k_x q_{j,x}) p_{j,x}$ a priori does not vanish. However, as the simulations show, it is of the same order as $\Sigma_{j=1}^{N} \cos(k_x q_{j,x}) \sin(k_x q_{j,x})$, which is also small and non-vanishing due to the uneven spacing of the particles.

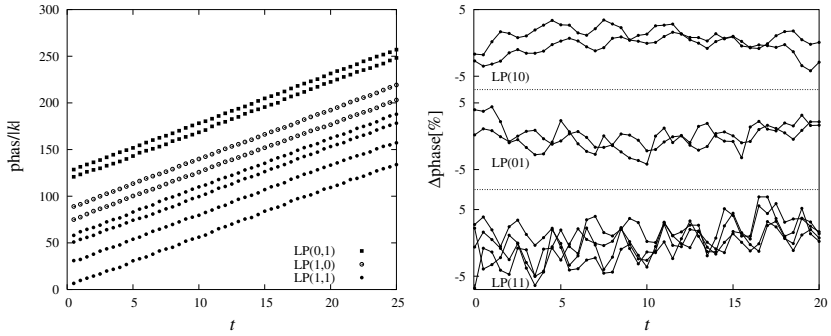

Fig. 9. Rotations of various LP pairs for the 780-disk system of Fig. 1. Left: Time dependence of the phase. For clarity, the phases for different modes are separated by multiples of $2\pi/|k_{\mathbf{n}}|$. Right: The fluctuations around the constant velocity (in percent of 2π). For details we refer to the main text.

Next, we consider the dynamics for the general case of a $2d$-fold degenerate LP(**n**) space. As explained in Section 4, an LP(**n**) space is defined by a spanning set of d longitudinal modes, $\varphi_1^{\mathrm{L}}, \ldots, \varphi_d^{\mathrm{L}}$, and d P-modes, $\varphi_1^{\mathrm{P}}, \ldots, \varphi_d^{\mathrm{P}}$, where each pair $(\varphi_k^{\mathrm{L}}, \varphi_k^{\mathrm{P}})$ is an LP pair. The following description is valid for any type of boundary conditions:

Dynamics in LP(n). The dynamics in LP(**n**), when restricted to a two-dimensional subspace spanned by an LP pair

$$\mathrm{Span}\{\varphi_k^{\mathrm{L}}, \varphi_k^{\mathrm{P}}\},$$

is a two-dimensional rotation at a constant angular velocity $\pm\omega_{\mathbf{n}}$, where $\omega_{\mathbf{n}} = v k_{\mathbf{n}}$, with v independent of **n**.

Example 5. The LP dynamics for higher-dimensional spaces is illustrated in Fig. 9. In the following we concentrate on LP(1,1). This space has dimension 8, that is four LP pairs. Generically, a measured mode has a non-vanishing projection onto all four LP pairs, and four different phases can be defined. The four time series of phases for LP(1,1) in Fig. 9 belong to different projections of the *same* mode.

6. INFLUENCE OF GEOMETRY AND SYSTEM SIZE

In this section, we study what influence the density, aspect ratio, and boundary conditions have on c_{T}, c_{L}, and v. The density dependence is significant. Unfortunately, we do not have any explanation for this fact. In particular, comparisons with the sound velocity,[25] with the mean free

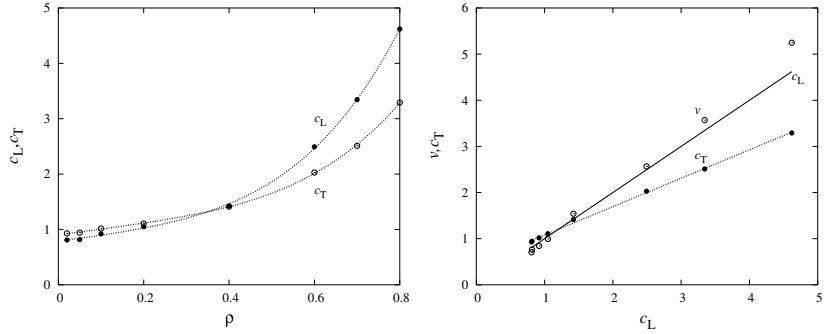

Fig. 10. Slopes of the transverse and longitudinal branches c_T and c_L of Fig. 5, and of phase velocity v. The simulations are for a system containing $N=780$ particles in a rectangular periodic box with a fixed aspect ratio $L_y/L_x=0.867$. Left: c_T and c_L as a function of the particle density ρ. The smooth lines are polynomial fits added to guide the eyes. Although the fits have no theoretical basis, we provide the fit parameters for convenience: $c_L=0.790+0.970\rho+0.785\rho^2+6.24\rho^4$, and $c_T=0.902+1.050\rho-0.053\rho^2+3.85\rho^4$. Right: Almost linear relations between all three quantities.

path, and with similar quantities, do not suggest simple relationships. Thus, these questions have to await further studies.

The results of our simulations are summarized in Fig. 10. In the left panel, c_L and c_T, defined in Section 2, are shown as functions of ρ, and on the right panel v and c_T are plotted as functions of c_L. There are two observations which are of interest: First, as seen in the left panel, c_T and c_L cross for lower densities. Thus, the intuitively natural conjecture, $c_L \geqslant c_T$, is not supported by the numerical evidence. Second, the three "velocities" c_T, c_L, and v are almost linearly related. In particular, the phase velocity v agrees rather well with c_L for fluid densities $\rho<0.6$ (see the full line in the right panel of Fig. 10), thus lending support to referring to the curves $\lambda(k)$ as "dispersion relations".

On the left panel of Fig. 11 we plot the longitudinal and transverse dispersion relations for a moderately-dense gas with a density $\rho=0.4$. The full and open points are for systems with periodic and reflecting boundaries, respectively. In all cases, λ was determined from the lowest step of the Lyapunov spectrum for the system, for which the aspect ratio varied between 0.5 and 1, and the particle number between 400 and 800. The figure demonstrates that periodic and reflecting boundary conditions give the same $\lambda(k)$. We have experimentally verified (but not shown here) that the same is true also for larger and lower densities.

The situation becomes a little more complicated when we consider the dependence of the slopes, c_L and c_T, on the aspect ratio A, as we do in

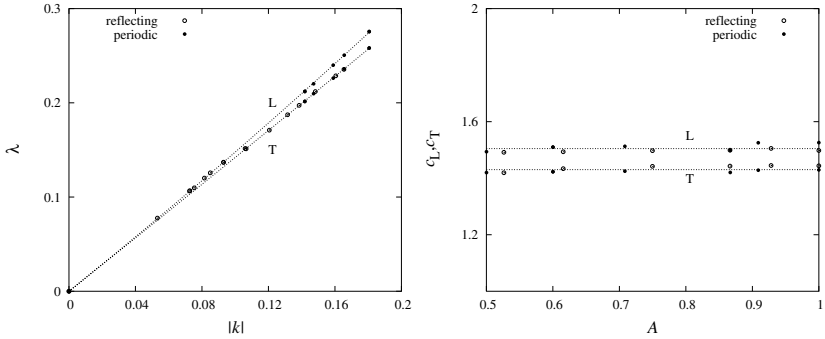

Fig. 11. Simulation results for a hard-disk gas with a density $\rho = 0.4$. The full and open points refer to periodic and reflecting boundary conditions, respectively. Left: The smallest positive Lyapunov exponent for T- and L-modes, respectively, as a function of the wave-number k. The curves for periodic and reflecting boundary conditions agree. To the second order in k, a fit to the data gives $c_L = 1.422k + 0.55k^2$ and $c_T = 1.412k + 0.086k^2$. Right: The slopes, c_L and c_T, are plotted as a function of the aspect ratio A of the simulation box. For a given A we compare points with the same k to eliminate the influence of the nonlinearity of the dispersion relations. This means that for periodic boundaries the linear extensions of the simulation box, L_x and L_y, are twice those of the respective reflecting box. The data for periodic and reflecting boundaries agree to within numerical accuracy.

the right panel of Fig. 11. The dispersion curves are not strictly linear in k, as we have pointed out already in a footnote in Section 2. A fit to the points in the left panel of Fig. 11 reveals that the term proportional to k^2 is much larger for L than for T. To eliminate this nonlinearity in a comparison of the slopes for reflecting and periodic systems with a given A, modes with the same values for k[21] are used in the right panel of Fig. 11. With this precaution the figure demonstrates that the slopes of the dispersion relations do not depend on the boundary conditions in any significant way, as long as the box does not degenerate to a narrow channel.[23] Except for this particular case, the nonlinearity of the dispersion curves has no noticeable influence on the classification and description of the Lyapunov modes in this paper and has been accordingly ignored.

7. HYDRODYNAMIC EQUIVALENT OF THE MODES

There is a general expectation that the Lyapunov modes should be related to the hydrodynamic behavior of the system, and several papers

[21] The smallest wave number k for periodic boundaries is given by $2\pi/L$, where L is a dimension of the box. For reflecting boundaries, k is given by π/L, where L is an effective box size, namely the size reduced by a particle diameter σ.

Table V. Modulations of the Hydrodynamic Fields (Multiplicative Constants are Omitted)

mode	$\delta\xi$	$\delta\rho$	δu	δE
T	$\nabla \wedge A$	0	$\nabla \wedge A$	0
L	∇A	ΔA	∇A	ΔA
P	vA	0	∇A	A

point in this direction.[3–6] It should be noted, however, that none of these studies has reached a totally convincing interpretation, and, furthermore, it is obvious from this body of work that the LP-modes are more difficult to explain than the T-modes. Here, we add to this a simple calculation which might be helpful in the future: we determine how the modes perturb the hydrodynamic fields or, in other words, what would be the *hydrodynamic equivalent* of the modes we measure. The results, given in Table V, have quite a simple form, but do not reproduce the usual modes of hydrodynamics.

Consider a general transformation T of the one-particle phase space $\mu \equiv [0, L_x) \times [0, L_y) \times \mathbf{R}^2$ given by

$$T: \begin{cases} r \mapsto r' = r + \varepsilon\delta\xi(r, v) \\ v \mapsto v' = v + \varepsilon\delta\eta(r, v) \end{cases},$$

and f a probability density over μ. If ε is infinitesimal, then the new probability density is $f' = f + \varepsilon\delta f$, where

$$\delta f = -f\left(\nabla_r \cdot \delta\xi + \nabla_v \cdot \delta\eta\right) - \nabla_r f \cdot \delta\xi - \nabla_v f \cdot \delta\eta, \tag{13}$$

see Appendix B. Since we study equilibrium dynamics, we assume, furthermore, that f is the Boltzmann distribution.[22] By Section 3.3 we also have $\delta\eta = C\delta\xi$, and, therefore, (13) simplifies to

$$\delta f = -f\left(\nabla_r \cdot \delta\xi + C\nabla_v \cdot \delta\xi - Cv \cdot \delta\xi\right).$$

We define the variations of the three hydrodynamic fields (density ρ, momentum u, and energy E) by

$$\delta\rho(r) = \int dv\delta f(r, v), \quad \delta u(r) = \int dv\delta f(r, v)v, \quad \delta E(r) = \int dv\delta f(r, v)|v|^2.$$

[22] With $k_B T = 1$ as in the simulations.

For each of the three types of modes, one can compute these quantities as a function of the scalar modulation A introduced in (9). The results are given in Table V. Since $\Delta A = -k_{\mathbf{n}}^2 A$, we note that the scalar fields $\delta\rho$ and δE are proportional to the initial scalar modulation A. Note also that the energy field is only affected by the L and P-modes but not by the T-mode.

8. CONCLUSIONS

The picture developed in this paper is for two-dimensional hard disks, but the method is sufficiently geometric and general to allow easy extensions to other systems:

For example, the generalization to three-dimensional hard disks is straightforward. The existence of L- and T-modes for this case has been confirmed by computer simulation.[25] Recently, Lyapunov modes were also found for two-dimensional soft-particle systems interacting either with a Weeks-Chandler-Anderson potential[26] or a Lennard–Jones potential.[27,28] It would also be interesting to extend the work to, say, circular geometries. Another extension concerns linear molecules such as hard dumbbells in a periodic box.[1,11] In this case two qualitatively different degrees of freedom play a role, translation and rotation. The existence of modes has already been demonstrated in this case.

We have ended our wanderings through the rich landscape of Lyapunov modes. To summarize, we have carefully identified and analyzed the modes, giving a beginning of a theoretical classification. Furthermore, we have seen that the Lyapunov exponents and the phase velocity of the LP-modes seem to be functions of the density alone. In particular, they are practically independent of the aspect ratio of the box (and, where applicable, also insensitive to the boundary conditions).

APPENDIX A: TRAVELING WAVES OF LP DYNAMICS

We consider the LP(1, 0) space of a rectangular system with periodic boundary conditions, defined by the four spanning vectors

$$\varphi_{\sin}^{\mathrm{L}} = \begin{pmatrix} s_x \\ 0 \end{pmatrix}, \quad \varphi_{\cos}^{\mathrm{P}} = \begin{pmatrix} p_x \\ p_y \end{pmatrix} c_x, \quad \varphi_{\cos}^{\mathrm{L}} = \begin{pmatrix} c_x \\ 0 \end{pmatrix}, \quad \varphi_{\sin}^{\mathrm{P}} = \begin{pmatrix} p_x \\ p_y \end{pmatrix} s_x.$$

We take an initial tangent vector

$$\delta\xi_0 = a\varphi_{\sin}^{\mathrm{L}} + b\varphi_{\cos}^{\mathrm{P}}. \tag{A.1}$$

After a time $\tau = 2\pi/(4\omega_{\mathbf{n}})$, the vector is transformed to

$$\delta\xi_\tau = a\varphi^{\mathrm{P}}_{\cos} + b\varphi^{\mathrm{L}}_{\sin}. \tag{A.2}$$

Assume that a and b are more or less equal. Then (A.1) will resemble a sinus, with much "noise" due to the P component, while (A.2) will look more like a cosine. In the dynamics leading from (A.1) to (A.2) a kind of "traveling wave" is therefore visible, which seems to cover a distance $2\pi|k_{\mathbf{n}}|^{-1}$ in a time $2\pi\omega_{\mathbf{n}}^{-1}$, thus "moving" at velocity $v = \omega_{\mathbf{n}}/|k_{\mathbf{n}}|$. In actual simulations, we cannot expect typical vectors to have a phase difference of $\frac{\pi}{2}$ between their $\varphi^{\mathrm{L}}_{\sin}$ and $\varphi^{\mathrm{L}}_{\cos}$ components, as in our example. Therefore, the observed wave displacement as seen in refs. 24, 25 has the shape of "steps" in a space–time diagram, with an average slope equal to v.

APPENDIX B: TRANSFORMATION OF THE ONE-PARTICLE DISTRIBUTION

Let f be a given distribution. For $\Gamma \subset \mu$, we have

$$F(\Gamma) \equiv \mathrm{Prob}(\text{one particle } \in \Gamma) = \int_\Gamma dr\, dv f(r, v).$$

The transported probability F' is defined by $F'(\Gamma') = F(\Gamma)$, where $\Gamma' = T(\Gamma)$. We shall compute its density f'. In the integral

$$F(\Gamma) = \int_{T^{-1}(\Gamma')} dr\, dv\, f(r, v), \tag{B.1}$$

we change the variables to $(r', v') = T(r, v)$. To first order in ε, we have

$$T^{-1}: \begin{cases} r' \mapsto\ r = r' - \varepsilon\delta\xi(r', v') \\ v' \mapsto\ v = v' - \varepsilon\delta\eta(r', v') \end{cases},$$

so (B.1) becomes

$$F(\Gamma) = \int_{\Gamma'} dr'\, dv' \det\left[\mathrm{D}T^{-1}|_{r', v'}\right] f(r' - \varepsilon\delta\xi(r', v'), v' - \varepsilon\delta\eta(r', v')). \tag{B.2}$$

The determinant is

$$\det\left[\mathrm{D}T^{-1}|_{r', v'}\right] = \det \begin{pmatrix} \mathrm{Id} - \varepsilon \mathrm{D}_r \delta\xi & -\varepsilon \mathrm{D}_v \delta\xi \\ -\varepsilon \mathrm{D}_r \delta\eta & \mathrm{Id} - \varepsilon \mathrm{D}_v \delta\eta \end{pmatrix}\Bigg|_{r', v'}$$

$$= 1 - \varepsilon \left[\nabla_r \cdot \delta\xi + \nabla_v \cdot \delta\eta \right]_{r',v'}. \tag{B.3}$$

To first order in ε, we obtain with (B.2) and (B.3)

$$\begin{aligned} F(\Gamma) = F(\Gamma') \; & -\varepsilon \int_{\Gamma'} dr' dv' f(r', v') \left[\nabla_r \cdot \delta\xi + \nabla_v \cdot \delta\eta \right]_{r',v'} \\ & -\varepsilon \int_{\Gamma'} dr' dv' \left[\nabla_r f \cdot \delta\xi + \nabla_v f \cdot \delta\eta \right]_{r',v'}, \end{aligned}$$

which is equivalent to (13).

ACKNOWLEDGMENTS

Financial support from the Austrian Science Foundation (FWF), project P15348, and the Fonds National Suisse is gratefully acknowledged.

REFERENCES

1. Lj. Milanović, H. A. Posch, and Wm. G. Hoover, What is 'Liquid'? Understanding the states of matter, *Mol. Phys*. **95**:281–287 (1998).
2. H. A. Posch and R. Hirschl, Simulation of Billiards and of Hard-Body Fluids, in *Hard Ball Systems and the Lorenz Gas*, D. Szász, ed. Encyclopedia of the mathematical sciences Vol. 101, (Springer Verlag, Berlin, 2000).
3. J.-P. Eckmann and O. Gat, Hydrodynamic Lyapunov modes in translation-invariant systems, *J. Stat. Phys*. **98**:775 (2000).
4. S. McNamara and M. Mareschal, The Lyapunov spectrum of granular gases, *Phys. Rev. E* **63**:061306 (2001).
5. S. McNamara and M. Mareschal, On the origin of the hydrodynamic Lyapunov modes, *Phys. Rev. E* **64**:051103 (2001).
6. T. Taniguchi and G. P. Morriss, Boundary effects in the stepwise structure of the Lyapunov spectra for quasi-one-dimensional systems, *Phys. Rev. E* **68**:026218 (2003).
7. A. de Wijn and H. van Beijeren, Goldstone modes in Lyapunov spectra of hard sphere systems, *Phys. Rev. E* **70**:016207 (2004).
8. Ch. Forster, R. Hirschl, H. A. Posch, and Wm. G. Hoover, Perturbed phase-space dynamics of hard-disk fluids, *Physica D* **187**:294 (2004).
9. V. I. Oseledec, A multiplicative ergodic theorem. Lyapunov characteristic numbers for dynamical Systems, *Trudy Mosk. Mat. Obsc*. **19**:179 [*Moscow Math. Soc*. **19**:197 (1968)].
10. J.-P. Eckmann and D. Ruelle, Ergodic theory of chaos and strange attractors, *Rev. Mod. Phys*. **57**:617 (1985).
11. Lj. Milanović and H. A. Posch, Localized and delocalized modes in the tangent-space dynamics of planar hard dumbbell fluids, *J. Mol. Liquids* **96–97**:221 (2002).
12. Ch. Dellago, H. A. Posch, and Wm. G. Hoover, Lyapunov instability of hard disks in equilibrium and nonequilibrium steady states, *Phys. Rev. E* **53**:1485 (1996).
13. G. Benettin, L. Galgani, and A. Giorgilli, J.-M. Strelcyn, *Meccanica* **15**:21 (1980).
14. I. Shimada and T. Nagashima, A numerical approach to ergodic problem of dissipative dynamical system, *Prog. Theor. Phys*. **61**:1605 (1979).
15. N. Chernov, Construction of transverse fiberings in multi-dimensional semidispersed billiards, *Funct. Anal. Appl*. **16**:270–280 (1983).

16. M. Wojtkowski, Systems of classical interacting particles with non-vanishing Lyapunov exponents in *Lyapunov exponents (Oberwolfach, 1990)*, Lecture Notes in Math. Vol. 1486 (Springer, 1991).
17. L. Bunimovich, C. Liverani, A. Pellegrinotti, and Y. Suhov, Ergodic systems of n balls in a billiard table, *Commun. Math. Phys*. **146**:357 (1992).
18. N. Simányi and D. Szász, Hard ball systems are completely hyperbolic, *Ann. Math*. **149**:35–96 (1999).
19. N. Simányi, The complete hyperbolicity of cylindric billiard, *Erg. Th. Dyn. Syst*. (2002), **22**:281–302.
20. N. Simányi, Proof of the ergodic hypothesis for typical hard ball systems, *Ann. Henri Poincaré* **5**:203–233 (2004).
21. M. Wojtkowski, "Measure theoretic entropy of the system of hard spheres", *Ergod. Th. & Dynam*. **8**:133 (1988).
22. Ch. Dellago and H. A. Posch, Kolmogorov–Sinai entropy and Lyapunov spectra of a hard sphere gas, *Physica D* **240**:68 (1997).
23. Ch. Forster, D. Mukamel, and H. A. Posch, Hard disk in narrow channels, *Phys. Rev. E* **69**:066124 (2004).
24. Ch. Forster, R. Hirschl, and H. A. Posch, Analysis of Lyapunov modes for hard-disk systems, Proceedings of ICMP 2003.
25. R. Hirschl, Computer simulation of hard-disk systems: "Lyapunov modes" and stochastic color conductivity, diploma thesis, University of Vienna (1999).
26. Ch. Forster and H. A. Posch, Lyapunov modes for soft-disk fluids, *New J. Phys*. **7**, article 32 (2005).
27. G. Radons and H. Yang, Static and dynamic correlations in many-particle Lyapunov vectors, submitted to *Phys. Rev. Lett*. (2004).
28. H. Yang and G. Radons, Lyapunov instabilities of Lennard-Jones fluids, *Phys. Rev. E*, submitted (2004).